Comparison of 2D melting criteria in a colloidal system

Comparison of 2D melting criteria in a colloidal system

Patrick Dillmann, Georg Maret and Peter Keim

Fachbereich Physik, Universität Konstanz, D-78457 Konstanz, Germany

E-mail: peter.keim@uni-konstanz.de

Abstract
We use super-paramagnetic spherical particles which are arranged in a two-dimensional monolayer at a water/air interface to investigate the crystal to liquid phase transition. According to the KTHNY theory a crystal melts in thermal equilibrium by two continuous phase transitions into the isotropic liquid state with an intermediate phase, commonly known as the hexatic phase. We verify the significance of several criteria based on dynamical and structural properties to identify the crystal–hexatic and hexatic–isotropic liquid phase transitions for the same experimental data of the given setup. The criteria are the bond orientational correlation function, the Larson–Grier criterion, the 2D dynamic Lindemann parameter, the bond orientational susceptibility, the 2D Hansen–Verlet rule, the Löwen–Palberg–Simon criterion as well as a criterion based on the shape factor of Voronoi cells and Minkowski functionals. For our system with long-range repulsion, the bond order correlation function and bond order susceptibility work best to identify the hexatic–isotropic liquid transition and the 2D dynamic Lindemann parameter identifies unambiguously the hexatic–crystalline transition.

(Some figures may appear in colour only in the online journal)

1. Introduction

While the liquid to crystal transition in three-dimensional systems is usually a first order transition, the situation in two-dimensional systems is found to be more complex. While grain-boundary induced melting [1, 2] or condensation of geometrical defects [3, 4] suggest a first order phase transition, the theory of Kosterlitz, Thouless, Halperin, Nelson and Young [5–8] predicted a melting process via two continuous phase transitions with an intermediate phase. The intermediate phase appears due to the fact that the translational and orientational symmetries are broken at different temperatures. The first phase transition at temperature T_m is associated with destroying the discrete translational symmetry. The intermediate phase is named hexatic based on the remaining sixfold quasi-long-range orientational order. If the orientational symmetry is destroyed to a short-range one at temperature $T_i > T_m$ a second phase transition from the hexatic to the isotropic liquid occurs. According to the KTHNY theory the different symmetries are affiliated with the occurrence of different topological defects, namely dislocations and disclinations.

The first simulations of small systems of hard disks showed a single first order transition [9]. For increasing system size a first order transition with a short correlation length was ruled out but the data were compatible with a weak first order transition as well as a continuous scenario. Since a phase coexistence was reported in an equilibrated ensemble we would like to argue in favor of a weak first order scenario. Simulating larger systems with up to 4 million particles with the same computer code it was shown that a van der Waals loop, which is usually interpreted as a first order criterion, weakens with increasing system size [10]. But especially in small systems the existence of a van der Waals loop cannot be taken as the sole criterion since the size of the loop strongly depends on the boundary conditions and even systems which are known to have continuous transitions show a van der Waals loop [11]. Simulations of dipolar particles were consistent with KTHNY theory [12]. Whether a system melts via a first order or via KTHNY theory may

depend on the core energy of dislocation [13], a quantity which one can calculate *a priori* only in the dilute limit of dislocations where renormalization effects do not appear [14]. Binder *et al* pointed out that the KTHNY scenario may easily be preempted by a first order transition [15]. Recent large scale simulations of hard core particles reported a continuous transition between the crystal and the hexatic phase, but since a phase coexistence of hexatic and isotropic liquid was found, this transition was reported to be first order [16].

In experimental systems, the existence of the intermediate hexatic phase is well established [17–24], but the nature of the transition is debated as well. Indications of first order transitions are reported in a colloidal system with screened Coulomb interactions [17] and di-block copolymer systems [21, 22]. Like in simulations, a phase coexistence is usually interpreted as a first order signature. KTHNY theory is a melting theory starting from large single crystals, but of course a thermodynamic phase should be independent of the history of the matter and cooling and heating cycles should give the same results. Wang *et al* reported finding poly-crystalline domains during cooling in a system of diameter-tunable microgel spheres at finite cooling rates [25]. Indeed, the cooling rates have to be small such that critical fluctuations of the continuous order phase transition can switch the symmetry globally. In the present system of particles with dipolar interaction we found (within the given resolution of temperature) both transitions to be continuous during melting and freezing. If the cooling rate is very slow (keeping the system always in quasi-thermal equilibrium) we do observe large single crystal domains in the field of view [23] implying that KTHNY theory also holds for freezing. However, when cooling the system rapidly from the isotropic liquid to the crystalline state we find a poly-crystalline sample without a signature of a hexatic phase during crystallization [26]. But even if growing crystalline domains are found in a liquid environment shortly after a temperature quench one should not interpret them as liquid–crystal coexistence—simply because the system is far out of equilibrium. In the same sense one should be careful of taking poly-crystallinity solely as a signature of first order transition if the system is cooled at a finite rate.

This paper is organized as follows. After a short introduction about the long-range order of crystals in two dimensions, the melting theory developed by Kosterlitz, Thouless, Halperin, Nelson, and Young is summarized in section 2. In section 3 we introduce our experimental setup and how we realize a colloidal monolayer. The following sections 4–11 introduce several quantities to identify different thermodynamic phases in 2D and discuss the results for our colloidal system with dipolar particle interaction. Finally we summarize the advantages and disadvantages of the measures in section 12.

2. Crystals in two dimension and KTHNY

Since the work of Peierls [27, 28] and Mermin [29, 30] it is known that strictly speaking no crystals exist in systems with dimension $D < 3$. In general, the significance of fluctuations is increased if the dimension of a system is decreased. Crystal lattices with dimension $D < 3$ are thermally unstable due to long-wavelength phonon modes. As a consequence long-range translational order does not exist. In the case of $D = 2$ Mermin showed that the displacement autocorrelation function

$$\langle [\mathbf{u}(\mathbf{r}) - \mathbf{u}(\mathbf{r}')]^2 \rangle \sim \ln |\mathbf{r} - \mathbf{r}'| \qquad |\mathbf{r} - \mathbf{r}'| \to \infty \quad (1)$$

diverges logarithmically in the crystalline phase. The slow logarithmic divergence in 2D leads to crystals which possess only a quasi-long-range translational order. On the other hand the local crystalline orientation is preserved and a long-range bond orientational order exists. The absence of long-range translational order also affects the shape of the structure factor $S(\mathbf{q})$. In 3D the structure factor is characterized by a number of delta functions

$$S(\mathbf{q}) \sim \delta(\mathbf{q} - \mathbf{G}) \quad (2)$$

at the reciprocal lattice vectors $\mathbf{G}$ reflecting a non-diverging displacement $\mathbf{u}(\mathbf{r})$. In 2D the delta functions are replaced by a set of power-law singularities

$$S(\mathbf{q}) \sim |\mathbf{q} - \mathbf{G}|^{-2+\eta_{\mathbf{G}}(T)} \quad (3)$$

where

$$\eta_{\mathbf{G}}(T) = \frac{k_{\mathrm{B}} T |\mathbf{G}|^2 (3\mu_{\mathrm{R}} + \lambda_{\mathrm{R}})}{4\pi \mu_{\mathrm{R}} (2\mu_{\mathrm{R}} + \lambda_{\mathrm{R}})} \quad (4)$$

depends on the Lamé coefficients μ_{R} and λ_{R}.

As mentioned before, a 2D crystal is characterized by a long-range orientational and a quasi-long-range translation order. The KTHNY theory describes the melting of a hexagonal crystal by the appearance of thermally induced topological defects. The crystal–hexatic phase transition takes place at temperature T_{m} when thermally generated bounded pairs of dislocations which spontaneously appear in the crystal phase dissociate into single dislocations. While dislocations destroy the quasi-long-range translational order a quasi-long-range orientational order is preserved. The second phase transition, hexatic–isotropic liquid, at $T_{\mathrm{i}} > T_{\mathrm{m}}$ occurs when dislocations are separated into free disclinations. Disclinations destroy the remaining quasi-long-range orientational order so that in the isotropic liquid both the translational and orientational orders are short range.

By identifying the kind of translational and orientational order at a given temperature T the state of the system can be defined and thus the phase transition points. The nature of the order is marked by a different behavior of the density–density correlation function $g_{\mathbf{G}}$ and bond orientational correlation function g_6. The density–density correlation function is given by

$$g_{\mathbf{G}}(r = |\mathbf{r}_k - \mathbf{r}_l|) = \langle \rho^*(\mathbf{r}_k) \rho(\mathbf{r}_l) \rangle \quad (5)$$

where $\rho(\mathbf{r}_k) = e^{i\mathbf{G}\mathbf{r}_k}$ is the translational order parameter of particle k located at position $\mathbf{r}_k$. Practically the translational correlation function is rarely used to identify the melting temperature T_{m}. This is due to the fact that in a system with Mermin–Wagner fluctuations being present, the reciprocal lattice vector $\mathbf{G}$ is not easily determined due to the power-law

singularities of the structure factor. Especially in large systems it is numerically difficult to extract **G** unambiguously.

The bond orientational correlation function is defined by

$$g_6(r = |\mathbf{r}_k - \mathbf{r}_l|) = \langle \psi_6^*(\mathbf{r}_k)\psi_6(\mathbf{r}_l) \rangle \tag{6}$$

with the sixfold bond orientational order parameter

$$\psi_6(\mathbf{r}_k) = \frac{1}{n_l} \sum_{i=1}^{n_l} e^{i6\theta_{kl}} \tag{7}$$

where n_l is the number of nearest neighbors of particle k and θ_{kl} is the angle between the bond of particles k and l and an arbitrary but fixed reference axis. Here the $\langle \ \rangle$ brackets correspond to an ensemble average. The long-range orientational order in a crystal is expressed in a long-range bond orientational correlation function $\lim_{r\to\infty} g_6(r) \neq 0$ whereas an algebraic decay of the density–density correlation function $g_G(r) \sim r^{-\eta_G(T)}$ reflects the quasi-long-range translational order. The hexatic phase is characterized by an algebraic decay of $g_6(r) \sim r^{-\eta_6(T)}$ (quasi-long-range orientational order) with an exponent

$$\eta_6(T) = \frac{18k_B T}{\pi F_A} \tag{8}$$

depending on Frank's constant F_A. The short-range translational order on the other hand leads to an exponential decay of $g_G(r) \sim e^{-r/\xi_G(T)}$ with $\xi_G(T)$ being the translational correlation length. In the liquid regime of the phase diagram the orientational order is short range too, and the correlation function decays as $g_6(r) \sim e^{-r/\xi_6(T)}$ where $\xi_6(T)$ is the orientational correlation length.

In addition to the predictions of the KTHNY theory different criteria have been proposed to identify the phase transitions. Whereas Wang *et al* [25] tested various 2D freezing criteria in poly-crystalline samples of microgel particles we do so in mono-crystalline samples of dipolar particles. We verify the adaptability of the bond order correlation function, the Larson–Grier criterion, the Lindemann parameter, the bond orientational susceptibility, the 2D Hansen–Verlet rule, the 2D Löwen–Palberg–Simon criterion, the shape factors and the Minkowski functionals on the melting transitions.

3. Experimental system

The experimental system is described in detail in [31]. It consists of a 2D colloidal monolayer of spherical polystyrene spheres with diameter $d = 4.5$ μm suspended in water and sterically stabilized with the surfactant sodium dodecylsulfate. Nanoparticles of Fe_2O_3 are embedded homogeneously in the polystyrene spheres and are responsible for the super-paramagnetic behavior and a relatively large mass density of 1.5 g cm^{-3}. Therefore the particles are confined by gravity at a water/air interface formed by a droplet which is suspended by surface tension in a top sealed cylindrical hole (6 mm diameter) of a glass plate. An external magnetic field **H** perpendicular to the water/air interface induces a magnetic moment $\mathbf{M} = \chi\mathbf{H}$ in each particle causing a repulsive dipole–dipole pair interaction E_{magn} between them.

The dimensionless interaction parameter Γ which is given by the ratio of the magnetic versus thermal energy

$$\Gamma = \frac{E_{magn}}{k_B T} = \frac{\mu_0}{4\pi} \frac{(\chi\mathbf{H})^2(\pi\rho)^{3/2}}{k_B T} \propto T_{sys}^{-1} \tag{9}$$

is equivalent to an inverse system temperature. Under the conditions of temporally constant ambient temperature T and 2D particle density ρ the system temperature depends only on the magnetic field. As a result the system temperature can be easily adjusted by simply changing the strength of the magnetic field **H**.

An inhomogeneous distribution of the particles within the sample would induce a gradient in the system temperature causing a spatial dependence of the phase transition. Therefore it is crucial to align the water/air interface absolutely planar and horizontally. For this purpose several computer controlled regulation loops have been installed to adjust the interface and keep it temporally constant. A monochrome CCD camera is used to observe the particles by video microscopy. The field of view (1158 × 865 μm^2) contains ≈9000 particles whereas the whole system includes ≈250 000 particles. During data acquisition the coordinates of the particles in the field of view are determined *in situ* every ≈2 s over a period of 25 min by digital image processing with an accuracy of about 50 nm. In this way the phase space information is accessible on all relevant length and time scales. A crystal is melted by stepwise increasing the system temperature via a reduction of the magnetic field. In the range of the phase transitions the interaction parameter was changed in small steps with an increment of $\Delta\Gamma \approx 0.25$. After each modification of the interaction parameter the system was equilibrated for about a day. Figure 1 shows images of the colloidal monolayer in the crystalline (left) and isotropic fluid (right) phases.

4. Orientational correlation function

As a key quantity of KTHNY theory, figure 2 shows the bond orientational correlation function for temperatures in the crystalline, hexatic and isotropic liquid regimes. The evaluation of $g_6(r)$ includes a time average over several particle configurations in addition to the ensemble average. The bond correlation function stays finite for interaction parameters $\Gamma > \Gamma_M = 60$ in the crystalline phase. An algebraic decay is observed for $\Gamma = 59.6$ and 59.3 so that the crystalline–hexatic phase transition takes place between $\Gamma = 60$ and 59.6. In the liquid state ($\Gamma = 47.6$ and 39.5) the decay of $g_6(r)$ is exponential. This behavior is in accordance with the predictions of the KTHNY theory and reconfirms previous experimental results [19, 20, 23] for the given system. The hexatic–isotropic transition can be determined by investigation of the goodness-of-fit statistics of algebraic or exponential decay [23]. In principle one could also determine the hexatic–crystalline transition by investigating the slope of $g_6(r)$ in a log–log plot but it is numerically not very precise to distinguish between a small but finite and a zero slope decay. From $g_6(r)$ one can also extract two diverging quantities:
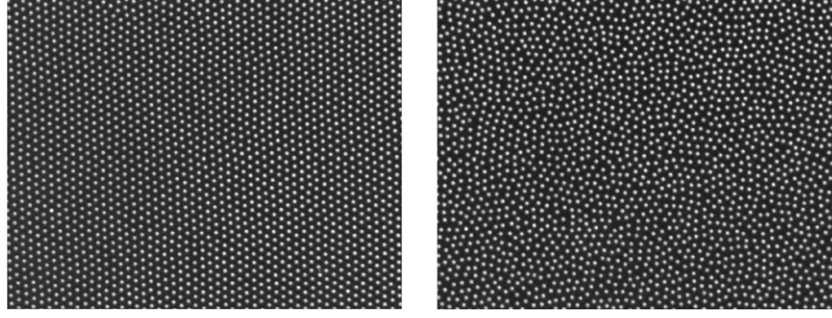
Figure 1. Image section of the CCD camera of a monolayer of colloidal particles. For high magnetic fields the particles arrange in a crystal (left) and for low magnetic field particles form a fluid (right). The images are a quarter in size of the full field of view (about $580 \times 430\ \mu m^2$). The hexatic phase is hardly distinguishable from the isotropic phase solely by eye and is not shown here.
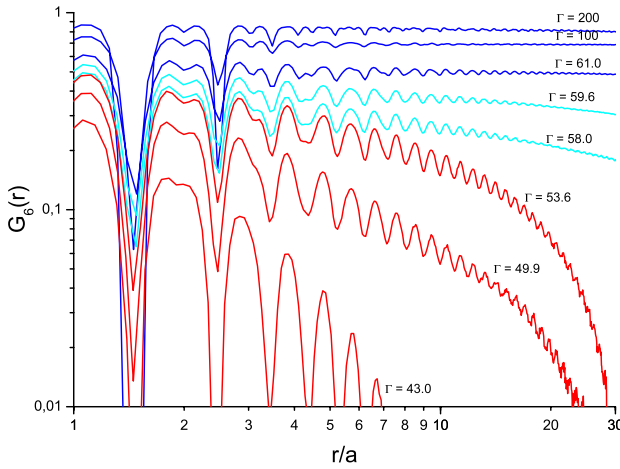
Figure 2. Orientational correlation functions $g_6(r)$ (in units of particle distances a) for different interaction parameters Γ. For $\Gamma \geq 60$, $g_6(r)$ reflects the long-range order of a crystal (upper three curves) while in the hexatic phase an algebraic decay is observed (the two curves in the middle). An exponential decay is observed in the isotropic liquid (lower three curves).

the orientational correlation length diverges at Γ_i and Frank's constant diverges at Γ_m. In [23] we fitted both divergencies to extract critical exponents but the transition temperatures were not taken as fitting parameters but used as an input. Otherwise fitting the transition temperatures to a single sided divergence in a finite field of view always overestimates the transition points by a few per cent.

5. Local bond order by Larson–Grier

To get insight into the local symmetry we focus on the magnitude of the local bond order parameter

$$m_{6_k} = |\psi_6(\mathbf{r}_k)|. \tag{10}$$

m_{6_k} is zero for perfect five- or sevenfold neighbored particles and one for perfect sixfold ones. It measures how the neighbors of particle k fit locally on a hexagonal lattice. To compare the local sixfold symmetry with neighboring

particles Larsen and Grier [32] investigated the magnitude of the projection of ψ_{6_k}

$$n_{6_k} = \left| \psi_{6_k}^* * 1/N_l \sum_l \psi_{6_l} \right| \tag{11}$$

to the mean local orientation field. It takes the second nearest neighbors into account and determines how the orientation of particle k fits into the orientation of its neighbor particles. Since it is a projection $n_{6_k} \leq m_{6_k}$ and $n_{6_k} + m_{6_k} \leq 2$. In [32] a unimodal distribution was found even if real space images showed a dilute liquid (or gas) phase and dense crystalline flakes implying an attractive interaction between particles to exist, whereas in [17] a bimodal distribution was reported next to the isotropic–hexatic as well as to the hexatic–crystalline transition. Particles in the m_6–n_6-plane with $m_6 + n_6 > 1$ (upper right corner) were identified to be crystal-like particles. Figure 3 shows the probability distribution for our purely repulsive system in the m_6–n_6-plane for several temperatures. The upper row shows plots in the crystalline phase, the second row shows plots of the hexatic phase and the two lowest rows are both from fluid phases. The absence of a bimodal distribution and the weak dependence of the local bond order field above and below Γ_i and Γ_m indicate continuous phase transitions. The third row shows that the local order in a 2D fluid is predominantly hexagonal, even far away from the phase transitions. Only at very high temperatures (low interaction strength) do most of the particles have $m_6 + n_6 < 1$, indicating that the local sixfold order up to the second shell is lost (lowest line). Since the dependence of the local bond order on the different phases is weak, it does not serve as a sharp criterion for phase transition temperatures.

6. Lindemann parameter

The Lindemann parameter is a well-known criterion in 3D to identify the melting point of crystalline structures. According to Lindemann [33] the melting of a crystal takes place if the thermal energy leads to displacements of atoms in relation to their equilibrium lattice sites which are in the range of one-half of the interatomic distance. The Lindemann
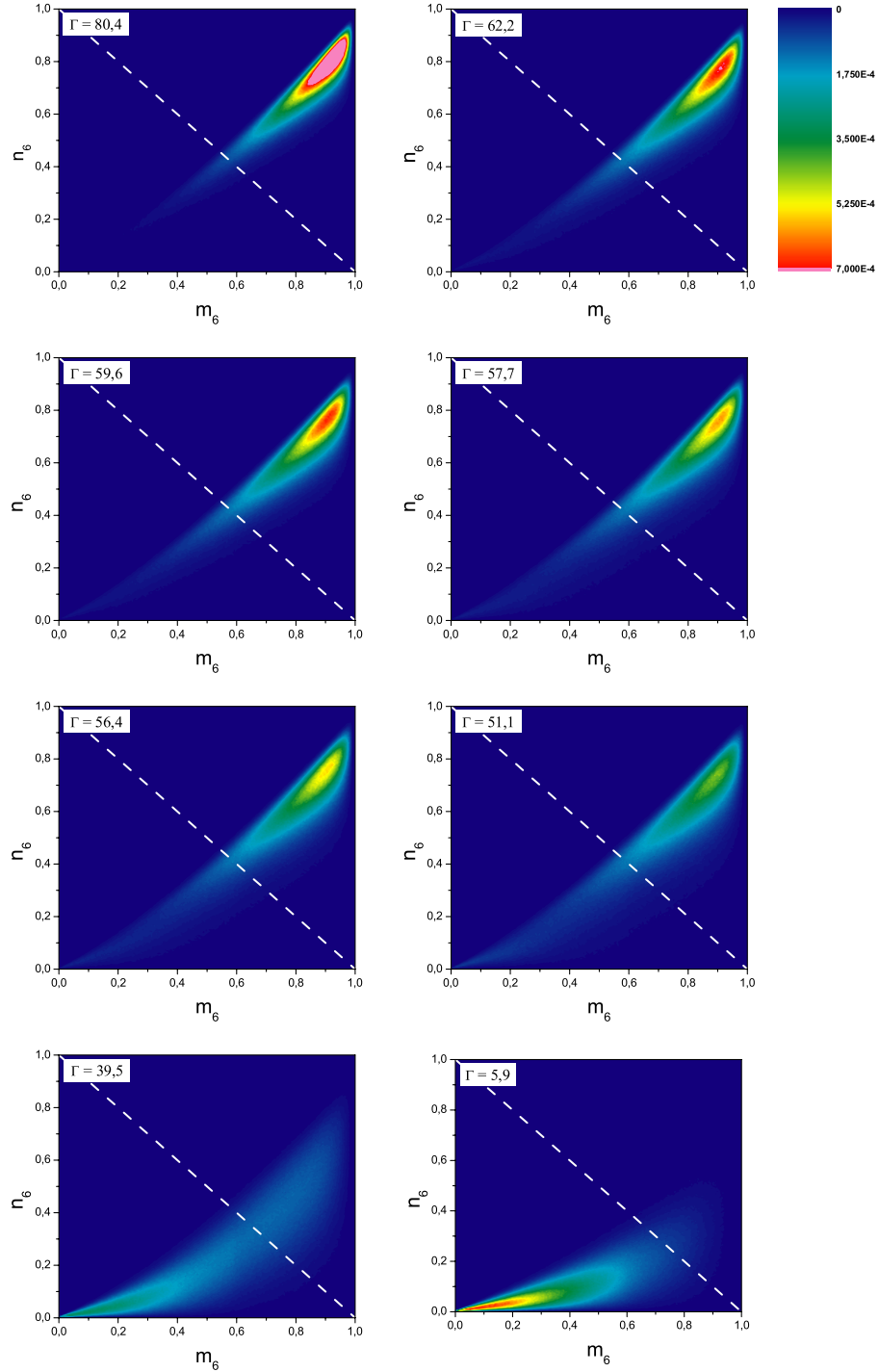
Figure 3. Probability distribution of the magnitude of the local bond order parameter m_6 versus the magnitude of the projection of ψ_6 to the mean of nearest neighbors n_6. The probability distribution changes continuously at both phase transitions and no bimodal distribution can be found.

criterion was modified by Gilvarry [34] by considering the root-mean-square amplitude of thermal vibrations. He suggested that the melting process is initiated when the ratio of the root-mean-square amplitude and the interatomic distance reaches a critical value of approximately 0.1.

The Lindemann criterion in this form is inapplicable in 2D. Due to the long-wavelength phonon modes the Lindemann parameter diverges in a crystal as well as in a

liquid. Bedanov *et al* [35] introduced a melting criterion for 2D

$$\gamma_{\mathrm{m}} = \frac{\langle |\mathbf{u}_j - \mathbf{u}_{j+1}|^2 \rangle}{a^2} \qquad (12)$$

analogous to the Lindemann parameter in 3D based on the displacement $\mathbf{u}_j$ of particle j with respect to its nearest neighbors $j + 1$ and normalized to the average inter-particle
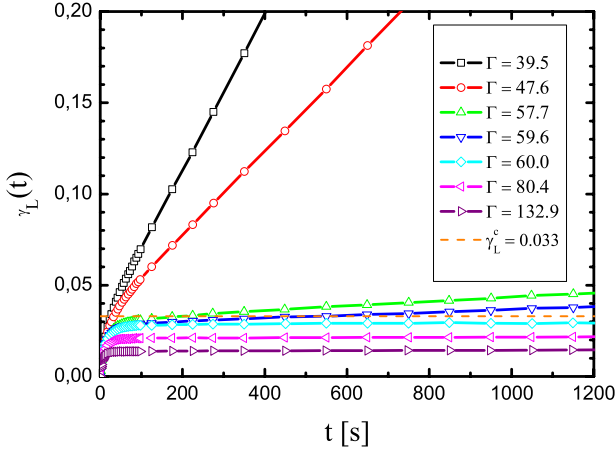
Figure 4. The dynamic Lindemann parameter stays finite in the crystal phase and diverges in the hexatic and isotropic liquid states. Γ increases from top to bottom with the same order as in the legend.

Figure 5. The bond orientational susceptibility for interaction parameters in the isotropic liquid, hexatic and solid states. The maximum of the peak corresponds to the isotropic liquid phase transition.

distance a. Zahn *et al* [19] generalized equation (12) to a dynamic Lindemann parameter

$$\gamma_L(t) = \frac{\langle [\Delta \mathbf{u}_i(t) - \Delta \mathbf{u}_{i+1}(t)]^2 \rangle}{2a^2} \quad (13)$$

where $\Delta \mathbf{u}(t) = \mathbf{u}(t) - \mathbf{u}(t=0)$. The crystal–hexatic phase transition can be determined by the long-time behavior of $\gamma_L(t)$. The Lindemann parameter $\gamma_L(t \to \infty)$ diverges in the hexatic and isotropic liquid phases whereas in a crystal $\gamma_L(t \to \infty)$ stays finite below a critical value $\gamma_L^c = 0.033$.
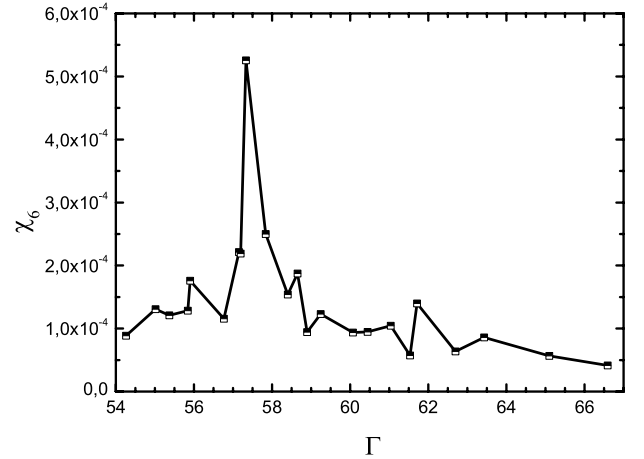
The Lindemann parameter $\gamma_L(t)$ is shown in figure 4 for different interaction parameters Γ. As expected, $\gamma_L(t)$ converges in a crystal ($\Gamma \geq 60$) to a finite value $< \gamma_L^c$ but diverges in the hexatic phase ($\Gamma = 59.6$ and 57.7) and isotropic liquid state ($\Gamma = 53.7$, 49.6 and 39.5). According to the behavior of the Lindemann parameter the crystal–hexatic transition occurs in the range between $\Gamma = 60.0$ and 59.6. This result is in excellent agreement with the predictions of the KTHNY theory and the determination of the crystal–hexatic phase transition obtained with the help of the bond orientational correlation function g_6. If grain boundaries are visible due to finite cooling rates or density gradients in the sample, the dynamic Lindemann parameter is not finite for the crystalline state. However, for a mono-crystalline sample it acts as a very sensitive tool to determine the crystal–hexatic phase transition temperature Γ_m.

7. Bond orientational susceptibility

The hexatic–isotropic liquid phase transition is associated with fluctuations of the orientational order parameter ψ_6. The fluctuations can be quantified by the bond orientational susceptibility

$$\chi_6 = A(\langle |\Psi_6^2| \rangle - \langle |\Psi_6| \rangle^2) \quad (14)$$

where $\Psi_6 = 1/N \sum_{k=1}^{N} \psi_6(\mathbf{r}_k)$ is the global bond orientational order parameter of the N particles included in a system with size A. The bond orientational susceptibility increases
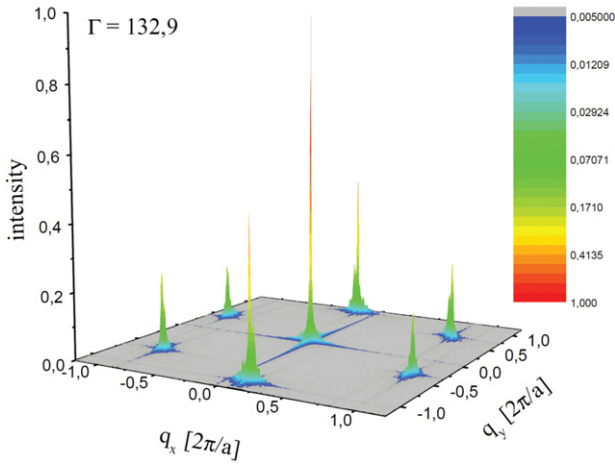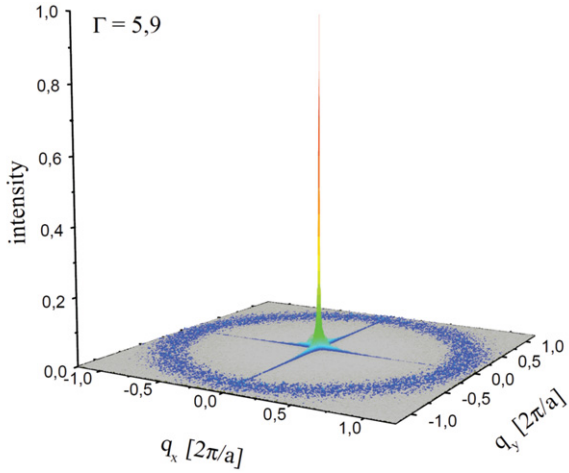
dramatically if the temperature reaches the point of the hexatic–isotropic liquid phase transition at Γ_i [36]. Here an increase of χ_6 is observed independently of whether the system approaches the transition point from the liquid phase $\Gamma \to \Gamma_i^-$ or from the hexatic phase $\Gamma \to \Gamma_i^+$. This behavior of the bond orientational susceptibility simplifies the identification of the hexatic–isotropic liquid phase transition in comparison with the previously mentioned method of the single sided divergence of the orientational correlation length $\Gamma \to \Gamma_i^-$. In figure 5 we see a sharp increase of χ_6 at $\Gamma = 57.5 \pm 0.5$. This result coincides with the value for the hexatic–isotropic transition obtained in [23]. The bond orientational susceptibility is a very sensitive tool to determine the transition temperature since we find a sharp increase from both sides of the peak (unlike e.g. the divergence of the orientational correlation length calculated from $g_6(\mathbf{r})$ where the divergence is single sided, see section 4 or [23]). In principle one could use the bond orientational susceptibility as a criterion for first order or second order transition [36]. A symmetric peak shape is predicted for second order or continuous transition whereas for first order transitions the limit of the susceptibility from above and below the transition should be different. Due to the limited temperature resolution in our data we do not want to overestimate this topic but at a first glance the data seem to be consistent with a second order transition.

8. Structure factor

The structure factor is another often used physical quantity to identify the freezing transitions. It is defined by

$$S(\mathbf{q}) = \frac{1}{N} \langle \rho(\mathbf{q}) \rho(-\mathbf{q}) \rangle \quad (15)$$

where the spatial Fourier transform of the number density $\rho(\mathbf{q})$ is given by

Figure 7. The isotropic structure factor $S(q)$ for different interaction parameters. The curves are shifted for reasons of clarity; Γ decreases from top to bottom with the same order as in the legend.

Figure 6. The structure factor $S(\mathbf{q})$ in the liquid phase (top) and crystalline phase (bottom). The rectangular cross in the center is an artifact due to the finite field of view.
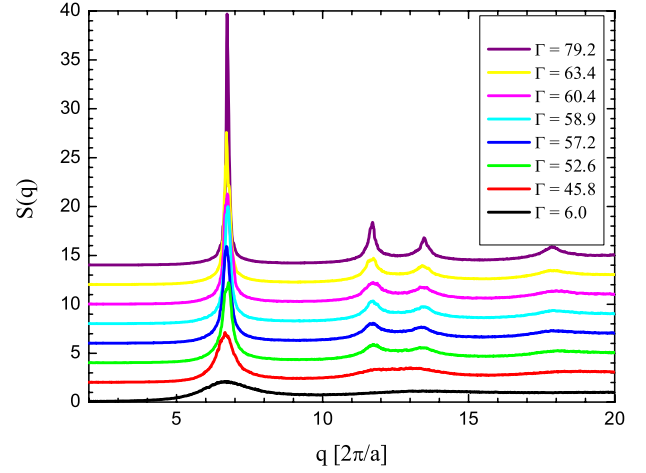
Figure 8. Amplitude of the first maximum of the structure factor $S(q_0)$. At the freezing point $\Gamma = 60$ the amplitude $S(q_0) \simeq 10$ for the system with long-range particle interaction. Two error-bars are shown in the isotropic and crystalline phases, calculated as the time average from different time steps at the given temperature.

$$\rho(\mathbf{q}) = \sum_{i=1}^{N} \exp(\mathbf{i}\mathbf{q}\mathbf{r}_i). \qquad (16)$$

Here $\langle \rangle$ denotes an ensemble average over N particles located at positions $\mathbf{r}_i$. Since we know the time dependent trajectories of the particles in the field of view we calculate the structure factor as function of time
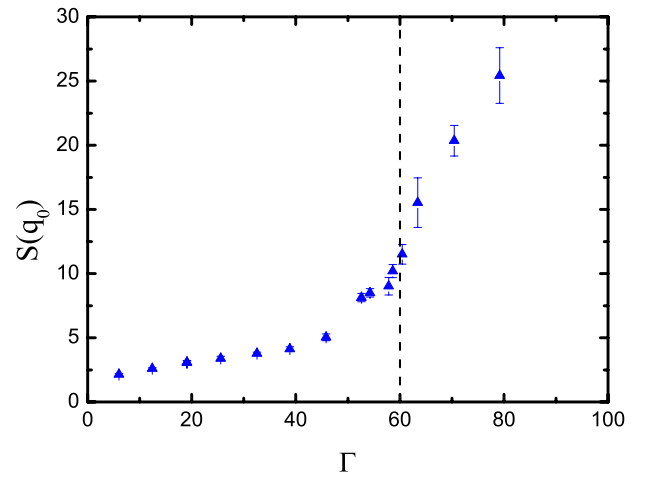
$$S(\mathbf{q}, t) = \frac{1}{N} \sum_{i=1}^{N} \sum_{j=1}^{N} \exp(\mathbf{i}\mathbf{q}\mathbf{r}_i(t)) \exp(-\mathbf{i}\mathbf{q}\mathbf{r}_j(t)) \qquad (17)$$

and determine $S(\mathbf{q}) = n_t^{-1} \sum_{t=1}^{n_t} S(\mathbf{q}, t)$ by a time average over $n_t > 70$ statistically independent particle configurations.

Figure 6 shows the structure factor $S(\mathbf{q})$ in the isotropic liquid and crystalline phases calculated from particle trajectories. Performing an azimuthal average gives the classical structure factor $S(q)$. Hansen and Verlet argued that freezing is associated with the amplitude $S(q_0)$ of the first maximum of the isotropic structure factor. A 3D liquid freezes when $S(q_0)$ exceeds a characteristic value of 2.85 [37]. The predictions of the characteristic value in

2D resulting from simulations vary from $S(q_0) = 4.4$ for particles with hard core and Coulomb interaction [38] to $S(q_0) = 5.75$ [39] for particles with r^{-12}-interaction. Figure 7 shows the temperature dependent isotropic structure factor $S(q)$ which is obtained by an angular average of the structure factor $S(\mathbf{q})$. The maximum of the isotropic structure factor $S(q_0)$ increases continuously as the temperature decreases (increasing interaction parameter Γ). Additionally the second maximum splits into two peaks which reflects an evolving hexagonal structure. As shown in figure 8, $S(q_0)$ rises slowly in the liquid and hexatic phases followed by a sharp rise after crossing the freezing point $\Gamma = 60$. The characteristic value is $S(q_0) \simeq 10$ and thus exceeds the estimated value by a factor of ≈ 2 for our system with long-range dipole–dipole interaction between the particles.

Another criterion about the global order is given by the line shape of the angular intensity of the structure factor.
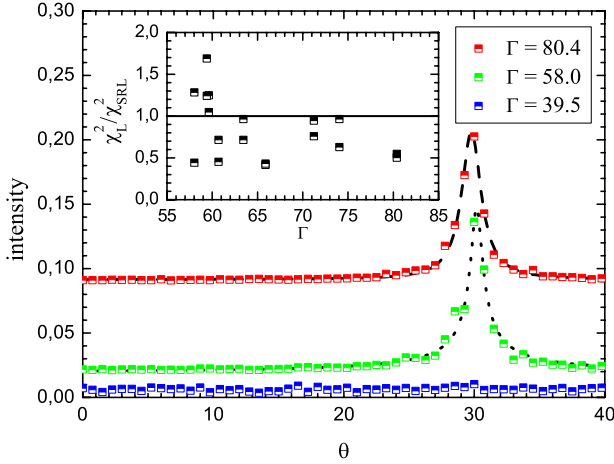
Figure 9. The line shape of the Bragg peak in the solid phase ($\Gamma = 80.4$) and the fit with a Lorentzian function (dashed line) and in the hexatic phase ($\Gamma = 58.0$) with an SQL function fit (dotted line). In the isotropic liquid ($\Gamma = 39.5$) the intensity shows no angular dependence. The curves are shifted for clarity. The inset shows the ratio of the goodness-of-fit statistics as a function of system temperature. Above $\Gamma_m = 60$ the Lorentzian function fits better and below Γ_m an SQL function fits better (except for the data-point at $\Gamma = 58$, see main text).

According to [40, 41] the line shapes of the Bragg peaks in the solid state are given by a Lorentzian function $S(\theta_0) = [(\theta_0 - \theta)^2 + \kappa^2]^{-1}$ where θ_0 is the angular position of the maximum of a Bragg peak, κ is the angular width of the Lorentzian function and the in-plane angle θ ranges from $\theta - \pi/6$ to $\theta + \pi/6$ because of the sixfold symmetry. In the hexatic phase a square-root Lorentzian (SRL) behavior $S(\theta_0) = [(\theta_0 - \theta)^2 + \kappa^2]^{-1/2}$ is expected. The line shapes of the Bragg peaks in the solid $\Gamma = 80.4$ and hexatic $\Gamma = 58.0$ phases are shown in figure 9 whereas in the isotropic liquid state $\Gamma = 39.5$ no angular dependence of the intensity is observed. To evaluate the behavior of the line shapes for different interaction parameters in the solid and hexatic phases a fit with a Lorentzian as well as a square-root Lorentzian function was executed. The line shape was determined on the basis of the reduced chi-square goodness-of-fit statistic χ^2 of the fits. The ratio χ_L^2/χ_{SRL}^2 of the Lorentzian and square-root Lorentzian reduced chi-square goodness-of-fit statistics is given in the inset of figure 9. The line shapes in the solid state are well reproduced by a fit with a Lorentzian function $\chi_L^2/\chi_{SRL}^2 < 1$ while in the hexatic phase a square-root Lorentzian function fits better, $\chi_L^2/\chi_{SRL}^2 > 1$. Only in the vicinity of the hexatic to isotropic liquid phase transition at $\Gamma_i = 57.5$ is this not the case for the data-point at $\Gamma = 58$. This might be due to the fact that below Γ_i the peaks should disappear and this data-point is too close to the isotropic transition to distinguish unambiguously between Lorentzian and square-root Lorentzian azimuthal shape.

9. The Löwen–Palberg–Simon criterion

Löwen *et al* [42] introduced a freezing criterion based on the dynamical properties of 3D systems. Their criterion
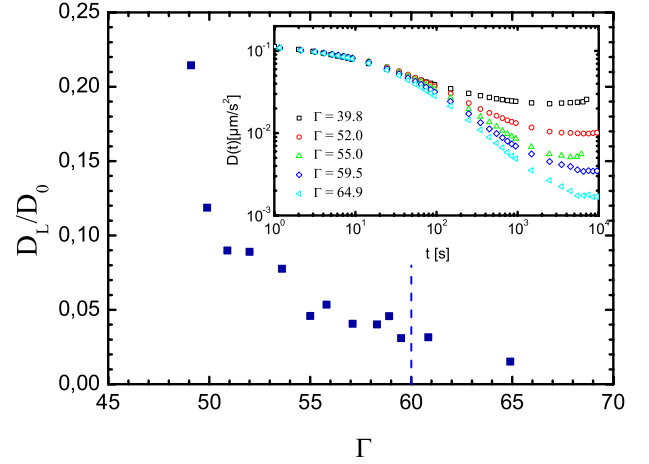

Figure 10. The temperature dependent ratios of the short-time versus long-time self-diffusion coefficients D_L/D_0. At the freezing point $D_L/D_0 \approx 0.03$ which has to be compared to a value of $D_L/D_0 = 0.086$ expected from simulation. The inset shows the time dependent diffusion constant calculated for different time-windows from the mean squared displacement.

states that a system starts to solidify if the ratio of the long-time self-diffusion coefficient D_L and the short-time self-diffusion coefficient D_0 reaches a critical value of 0.1. Brownian dynamics simulations of different pair potentials led to critical values in 2D between 0.072 (hard disks) and 0.099 (r^{-12} potential). In the case of a dipolar interaction a critical value of 0.086 was obtained [43]. The short-time and long-time self-diffusion coefficients are related to the mean-square displacement $\Delta r^2 = 1/N \sum_{i=1}^{N} [r_i(t) - r_i(0)]^2$ by the following equations:

$$D_0 = \lim_{t \to 0} \frac{\Delta r^2}{4t} \tag{18}$$

$$D_L = \lim_{t \to \infty} \frac{\Delta r^2}{4t}. \tag{19}$$

The ratios of the short-time and long-time self-diffusion coefficients for different interaction parameters are shown in figure 10. The critical value expected for the freezing point from simulation with a dipolar interaction cannot be reproduced. At the solid–hexatic phase transition $D_L/D_0 \approx 0.03$ which is a factor of three smaller compared to computer simulation for about 1000 dipolar particles [43]. In a poly-crystalline system of soft spheres a threshold of about $D_L/D_0 = 0.08$ is reported [25] supporting the simulations. Since we know that grain boundaries influence the 2D dynamical Lindemann parameter we expect a difference in the long-time diffusion coefficient between systems with and without grain boundaries. Additionally the short-time diffusion coefficient of particles at a water/air interface is larger compared to that of particles in the bulk. This together with the fact that grain boundaries are not visible in our field of view might explain the small value of 0.03 in our system. Zippelius [44] pointed out that the dependence of the ratio D_L/D_0 as a function of temperature may be used as a criterion for first and second order transition. First order transitions are characterized by a discontinuous jump at T_m whereas a
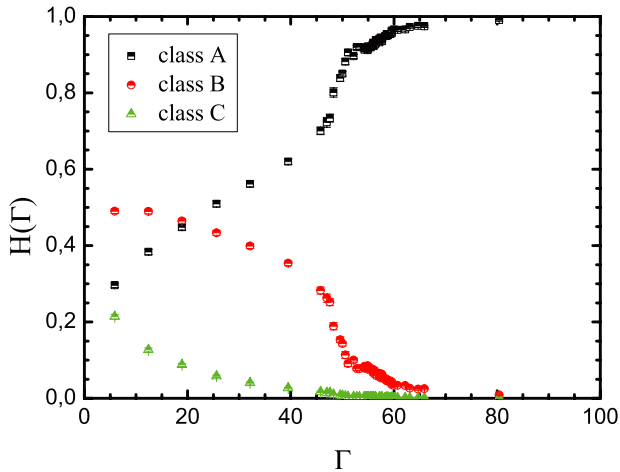
Figure 11. The fraction of particles assigning to three different classes A, B and C. The error-bars (calculated as the time average for different time steps at a given temperature) are smaller than the symbols.

Figure 12. The distribution of shape factors $P(\zeta)$ for different interaction parameters. The distribution changes from a bimodal shape for $\Gamma < 60.0$ to a unimodal shape in the solid, $\Gamma \geq 60$.

smooth change should be found for KTHNY-like behavior. Figure 10 shows a continuous variation as a function of system temperature. This again supports the result that our system melts according to KTHNY theory.

10. Shape factor

Moučka and Nezbeda introduced a shape factor ζ to analyze structural changes occurring for simulations of a hard disk system in the region of phase transitions [45]. The shape factor of particle i is defined as

$$\zeta_i = \frac{C_i^2}{4\pi S_i} \tag{20}$$

where C_i and S_i correspond to the perimeter and area of the Voronoi cell of the particle. The shape factor for a regular polygon with n edges is given by $\zeta_n^{\text{reg}} = n/\pi \tan(\pi/n)$. They observed that the distribution of the shape factor $P(\zeta)$ becomes bimodal near the freezing point. The distribution in the liquid state is broad and the maximum is located at relatively high ζ-values whereas in the solid a sharp distribution with a maximum near the value of a regular hexagon, $\zeta = 1.03$, is given. This behavior is explained by the evolution from different types of cells which are also distorted in the liquid to more regular hexagonal cells in the solid. Reis *et al* [46] classified the particles of a granular fluid into three classes according to their shape factors. Particles with $\zeta < \zeta_{\min}$ belong to class A, particles with $\zeta_{\min} < \zeta < \zeta_u$ belong to class B and particles with $\zeta > \zeta_u$ belong to class C where $\zeta_{\min} = 1.159$ and $\zeta_u = 1.25$. If the numbers of particles in classes A and B were equal they observed the transition from a liquid to an intermediate phase (coexistence or hexatic phase could not be evaluated). Approaching the freezing point a sharp decline of the number of class B particles occurred in the intermediate phase. After crossing the freezing point the number of class B particles decreased much more moderately in comparison with the intermediate phase.
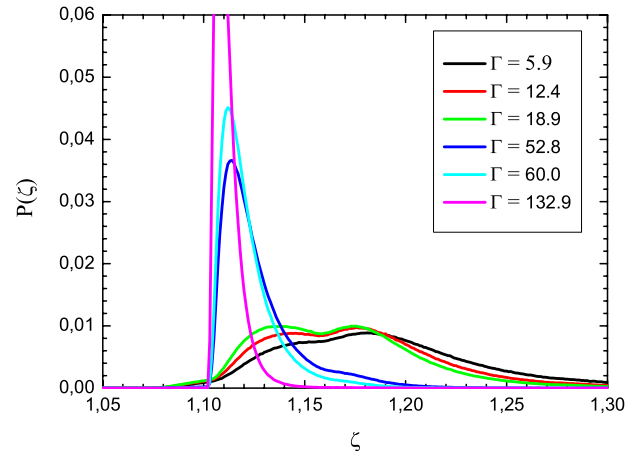
Using the classification procedure described in [46] we obtain an identical value for $\zeta_{\min}$ and a slightly deviating value $\zeta_u = 1.22$. In accordance with the granular system the slope of the fraction of particle class B changes at the freezing point as shown in figure 11. On the other hand the fractions of classes A and B are equal at $\Gamma \approx 20$ far away from the isotropic liquid–hexatic phase transition. We ascribe this different behavior to the structural changes which are less pronounced at the phase transitions compared to the hard disk or granular systems. This can been seen in figure 12 where even deep in the liquid state at $\Gamma = 5.9$ a bimodal distribution $P(\zeta)$ instead of a flat one exists. This indicates that in the liquid as well as in the crystalline state a hexagonal configuration of the particles is preferred. This assumption is confirmed by the fact that more than 50% of the particles at $\Gamma = 5.9$ are still sixfold coordinated. For our thermal system with long-range interaction, the phases are not identified unambiguously using shape factors.

11. Minkowski functionals

In addition to the previously described criteria we tested tentatively whether any hint for phase transitions could be derived from the behavior of Minkowski measures. Minkowski measures have been successfully adopted to specify spatial patterns, e.g. during spinodal decomposition [47], the evolution of galaxy clusters [48] or partial clustering in a 2D colloidal glass former [49]. Integral geometry offers a set of topological and geometrical descriptors (Minkowski functionals) to characterize spatial patterns. The operation of the Minkowski functional V on patterns $P, Q, \ldots$ has to obey three properties to be a morphological measure.

(i) Motion invariance: $V(gP + t) = V(P)$ for g and t being any rotation and translation.
(ii) Additivity: $V(P \cup Q) = V(P) + V(Q) - V(P \cap Q)$.
(iii) Continuity: a slight distortion of a pattern leads to a continuous change of V.
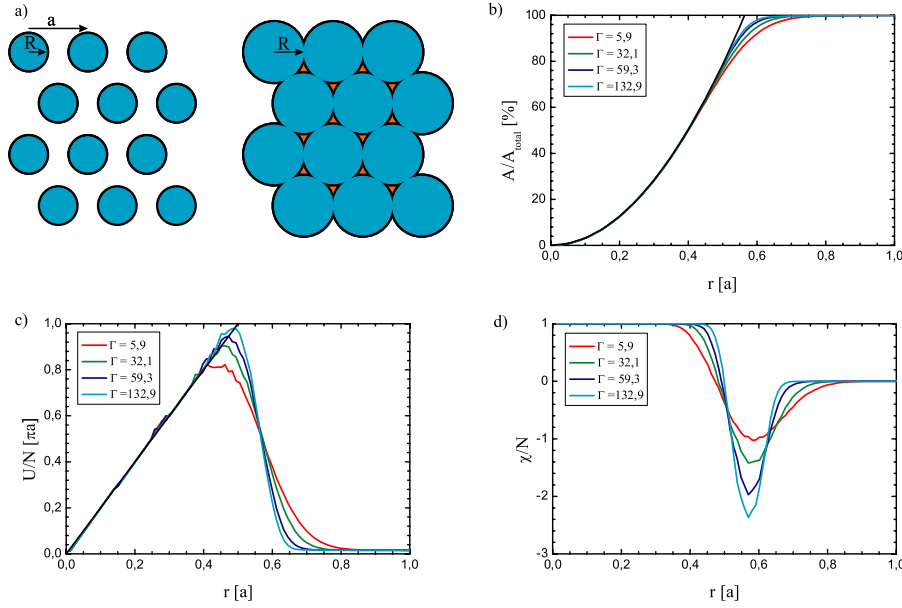
Figure 13. In 2D systems three independent Minkowski functionals exist which may be chosen as the surface area A, the circumference U and the Euler characteristic $\chi = N_a - H$.

According to Hadwiger [50] there exist exactly $D + 1$ linear independent Minkowski functionals in D dimension. In the case of $D = 2$ the Minkowski measures are related to the surface area A, the circumference U and the Euler characteristic $\chi = N_a - H$ which is given by the difference of the number of connected surfaces N_a and number of holes H.

We create a pattern for a single particle configuration by placing a cover disk with constant radius R at each particle position (see figure 13(a)). Morphological information about the particle configuration is then obtained by determining the Minkowski functionals as a function of cover radius R. As crystals in 2D possess sixfold symmetry we briefly describe the behavior of the Minkowski functionals for a perfect hexagonal lattice. The cover disks do not overlap for radius $0 \leq R < a/2$. The surface area and circumference are given by the area $A_d(R)$ and circumference $U_d(R)$ respectively of a cover disk times the number of cover disks N and the Euler characteristic is $\chi = N$. As requested by additivity for $a/2 \leq R < \sqrt{3}a/3$ the surface area is given by the sum of the area of the cover disks minus the overlapping areas which are connected with a slower increase of the surface area. Despite the radius being increased the circumference starts to decrease because the parts of the perimeters belonging to the overlapping areas of the disks are disregarded. The Euler characteristic becomes negative since the overlapping leads to only one connected surface while holes are formed. If the disk radius reaches a value of $R \geq \sqrt{3}a/3$ the whole area is covered and the circumference is equal to zero. The holes disappear, i.e. $\chi = 1$.

In figures 13(b)–(d) the three Minkowski functionals (b) surface area A, (c) circumference U and (d) Euler characteristic χ are shown for crystalline, hexatic and isotropic liquid systems. Note that A/A_{total}, U/N and χ/N are plotted. All Minkowski functionals reflect in principle the behavior which is characteristic for the hexagonal lattice. The deviations from the expected curves increase with the

inverse system temperature, i.e. with the thermal motion. The increase of the surface area is proportional to R^2 while the circumference is proportional to R and $\chi = 1$ as expected for small radii. The range where holes in the perfect hexagonal lattice exist is broadened to $0.35a \leq R \leq 0.8a$. For $R > 0.8a$ the full area is covered, $U/N = 0$ and $\chi/N \rightarrow 0$. No qualitative changes of the Minkowski functionals can be observed at the phase transitions. Changes of the Minkowski functionals which may emerge due to the emergence of defects cannot be identified due to their number density being quite small and due to strong thermal fluctuations of the particles. In contrast to a binary dipole–dipole system where structural heterogeneities have been quantified [49], Minkowski functionals are not applicable as order parameters to identify phase transition temperatures for our mono-disperse system.

12. Conclusion

In a two-dimensional system of colloids with repulsive dipolar interaction several criteria based on structural as well as dynamical quantities were compared to identify phase transitions. The criteria are the bond orientational correlation function, the Larson–Grier criterion, the 2D dynamic Lindemann parameter, the bond orientational susceptibility, the 2D Hansen–Verlet rule, the Löwen–Palberg–Simon criterion as well as the shape factor and the Minkowski functionals. A very sensitive tool to distinguish different symmetries is the bond order correlation function $g_6(\mathbf{r})$. The transition from algebraic decay to exponential decay marks the hexatic to isotropic fluid phase transition. The bond order parameter susceptibility provides similar results for the hexatic–isotropic transition and might be used as an alternative measure even applicable in poly-crystalline samples [25] which we may call 'poly-domain hexatic' or 'polyhexaline', since the measure is taken above T_m.

The counterpart of $g_6(\mathbf{r})$ is the density–density correlation function (equation (5)) for the hexatic to crystalline transition where the crossover from quasi-long-range to short-range translational order marks the symmetry breaking temperature. This quantity is rarely used in experiment since the reciprocal lattice vector is not precise enough to determine whether Mermin–Wagner fluctuations are present. Therefore we use a dynamic quantity, the mean-squared-displacement with respect to the nearest neighbors, namely the 2D dynamic Lindemann parameter, to identify the hexatic to crystalline transition. The 2D Lindemann parameter is a sensitive tool; it stays finite in the crystal but diverges in the fluid phase provided that the system is free of grain boundaries according to KTHNY theory. This should be the case for transitions with continuous character but on the experimental side substrate interaction, density and temperature gradients or large cooling rates may induce grain boundaries.

Since the local order in 2D systems is sixfold in both the fluid and the solid phases, local measures like the Larson–Grier criterion and the shape factor of Voronoi cells do not change significantly on crossing transition temperatures and are rather insensitive to global symmetry changes. This is at least true for our system with purely repulsive pair interaction where density differences do not appear in different phases.

The Hansen–Verlet rule modified for two-dimensional systems measures the height of the first peak of the structure factor. Values between $S(q_0) = 4.4$ and $S(q_0) = 5.75$ are reported in simulations. In our dipolar system we determined $S(q_0) \simeq 10$ at the melting point. A critical value might be given for individual systems but a universal value should be taken with care. This is the same for the ratio of the long-time versus short-time diffusion coefficient. In 3D systems the Löwen–Palberg–Simon criterion states that crystallization takes place at a critical value of 0.1. In 2D values between 0.072 and 0.099 are found in simulations, whereas in our system we found a value of 0.03. The discrepancies might be explained by grain boundaries as we do not know whether they were present in the simulations.

Finally we presented Minkowski functionals as topological measures to identify the phases. While we found the Minkowski functionals to be sensitive to locally heterogeneous distributions of particles in a binary mixture, they were rather insensitive to global symmetry changes and phase transitions.

Acknowledgment

References

[1] Chui S T 1983 *Phys. Rev.* B **28** 178–94
[2] Kleinert H 1983 *Phys. Lett.* A **95** 381–4
[3] Glaser M A and Clark N A 1993 *Adv. Chem. Phys.* **83** 543
[4] Lansac Y, Glaser M A and Clark N A 2006 *Phys. Rev.* E **73** 041501
[5] Kosterlitz J M and Thouless D J 1973 *J. Phys. C: Solid State Phys.* **6** 1181
[6] Nelson D R and Halperin B I 1979 *Phys. Rev.* B **19** 2457–84
[7] Halperin B I and Nelson D R 1978 *Phys. Rev. Lett.* **41** 121–4
[8] Young A P 1979 *Phys. Rev.* B **19** 1855–66
[9] Alder B J and Wainwright T E 1962 Phase transition in elastic disks *Phys. Rev.* **127** 359–61
[10] Mak C H 2006 *Phys. Rev.* E **73** 065104
[11] Alonso J J and Fernandez J F 1999 van der Waals loops and the melting transition in two dimensions *Phys. Rev.* E **59** 2659–63
[12] Lin S Z, Zheng B and Trimper S 2006 *Phys. Rev.* E **73** 066106
[13] Strandburg K J 1988 *Rev. Mod. Phys.* **60** 161–207
[14] Sengupta S, Nielaba P and Binder K 2000 *Phys. Rev.* E **61** 6294–301
[15] Binder K, Sengupta S and Nielaba P 2002 *J. Phys.: Condens. Matter* **14** 2323
[16] Bernard E P and Krauth W 2011 *Phys. Rev. Lett.* **107** 155704
[17] Marcus A H and Rice S A 1997 *Phys. Rev.* E **55** 637–56
[18] Kusner R E, Mann J A, Kerins J and Dahm A J 1994 *Phys. Rev. Lett.* **73** 3113–6
[19] Zahn K, Lenke R and Maret G 1999 *Phys. Rev. Lett.* **82** 2721–4
[20] Zahn K and Maret G 2000 *Phys. Rev. Lett.* **85** 3656–9
[21] Segalman R A, Hexemer A, Hayward R C and Kramer E J 2003 *Macromolecules* **36** 3272–88
[22] Angelescu D E, Harrison C K, Trawick M L, Register R A and Chaikin P M 2005 *Phys. Rev. Lett.* **95** 025702
[23] Keim P, Maret G and von Grünberg H H 2007 *Phys. Rev.* E **75** 031402
[24] Han Y, Ha N Y, Alsayed A M and Yodh A G 2008 *Phys. Rev.* E **77** 041406
[25] Wang Z, Ahmed A M, Yodh A G and Han Y 2010 *J. Chem. Phys.* **132** 154501
[26] Dillmann P, Maret G and Keim P 2008 *J. Phys.: Condens. Matter* **20** 404216
[27] Peierls R E 1934 *Helv. Phys. Acta* **7** 81–3
[28] Peierls R E 1935 *Ann. Inst. Henri Poincaré* **5** 177–222
[29] Mermin N D and Wagner H 1966 *Phys. Rev. Lett.* **17** 1133–6
[30] Mermin N D 1968 *Phys. Rev.* **176** 250–4
[31] Ebert F, Dillmann P, Maret G and Keim P 2009 *Rev. Sci. Instrum.* **80** 083902
[32] Larsen A E and Grier D G 1996 *Phys. Rev. Lett.* **76** 3862–5
[33] Lindemann F A 1910 *Phys. Z.* **609** 609–12
[34] Gilvarry J J 1956 *Phys. Rev.* **102** 308–16
[35] Bedanov V M, Gadiyak G V and Lozovik Yu E 1985 *Phys. Lett.* A **109** 289–91
[36] Weber H, Marx D and Binder K 1995 *Phys. Rev.* B **51** 14636–51
[37] Hansen J-P and Verlet L 1969 *Phys. Rev.* **184** 151–61
[38] Caillol J M, Levesque D, Weis J J and Hansen J P 1982 *J. Stat. Phys.* **28** 325–49
[39] Ramakrishnan T V 1982 *Phys. Rev. Lett.* **48** 541–5
[40] Aeppli G and Bruinsma R 1984 *Phys. Rev. Lett.* **53** 2133–6
[41] Davey S C, Budai J, Goodby J W, Pindak R and Moncton D E 1984 *Phys. Rev. Lett.* **53** 2129–32
[42] Löwen H, Palberg T and Simon R 1993 *Phys. Rev. Lett.* **70** 1557–60
[43] Löwen H 1996 *Phys. Rev.* E **53** R29–32
[44] Zippelius A, Halperin B I and Nelson D R 1980 *Phys. Rev.* B **22** 2514–41
[45] Moučka F and Nezbeda I 2005 *Phys. Rev. Lett.* **94** 040601
[46] Reis P M, Ingale R A and Shattuck M D 2006 *Phys. Rev. Lett.* **96** 258001
[47] Mecke K R and Sofonea V 1997 *Phys. Rev.* E **56** R3761–4
[48] Beisbart C, Valdarnini R and Buchert T 2001 *Astron. Astrophys.* **379** 412–25
[49] Ebert F, Maret G and Keim P 2009 *Eur. Phys. J.* E **29** 311–8
[50] Hadwiger H 1957 *Vorlesungen über Inhalt, Oberfläche und Isoperimetrie* (Berlin: Springer)